Effect of Applied Magnetic Field on Arcjet Thruster*†

Takeshi Miyasaka
Department of Aerospace Engineering, Nagoya University
Furo, Chikusa, Nagoya 464-8603 Japan
+81-52-789-3398
miyasaka@nuae.nagoya-u.ac.jp

Hiroshi Katsurayama
Department of Aeronautics and Astronautics, University of Tokyo
Hongo, Bunkyo, Tokyo 113-8656, JAPAN
+81-3-5841-6619
katsura@al.t.u-tokyo.ac.jp

Toshi Fujiwara
Department of Aerospace Engineering, Nagoya University
Furo, Chikusa, Nagoya 464-8603 Japan
+81-52-789-4400
toshi@nuae.nagoya-u.ac.jp

IEPC-01-130

Wall heat loss is a serious problem in arcjet thrusters. For the purpose of improving thermal efficiency, an analytical model taking account of applied magnetic field is proposed here. Steady MHD flows in an applied-field arcjet thruster are analyzed for several different geometries. The results show that the plasma is reasonably well accelerated to azimuthal direction by applied field where the input power is used in the form of Lorentz work, as is designed for performance improvement. The effects of applied field on thruster performance are evaluated in terms of thrust, thrust efficiency and anode heat loss caused by wall bombardment of electron from discharge current. It is discovered that thruster performance can be improved by applying a considerably intense magnetic field.

Introduction

Arcjet thrusters are promising propulsion devices, which heat up a gaseous propellant with Joule heating generated by an arc discharge from anode to cathode and then accelerates the propellant by expansion in nozzle. It is known that the arcjet has advantages of simple structure and relatively higher thrust density in comparison with electrostatic propulsion. However, the arcjet has a serious problem in the 1-10kW operating range at low voltage mode. Under this operating mode, the thrust efficiency is low because of increased heat flux to anode wall, caused by arc column attachment to anode. One method toward improvement would be that the arcjet is operated at high voltage mode, in order to prevent arc column attachment by stretching current streamlines to a more downstream part of thruster. This approach has been studied, using sophisticated numerical analyses and experiment[1]-[5]. Another improvement method may be that a part of total electric power input is applied in the form of azimuthal kinetic energy.

The acceleration mechanism of this method is shown in Fig.1. An axial magnetic field is applied by a solenoidal coil, being aligned coaxially with thruster axis. An azimuthal Lorentz force is generated by the interaction between this applied field and radial discharge current. This azimuthal force causes swirl acceleration of plasma: Consequently, the total power is given to plasma in the form of Lorentz work and Joule heating. Although some of kinetic energy is converted to static enthalpy of flow, it can finally be converted to axial kinetic energy through a solid nozzle. The hydrodynamic pressure, exerted on the solid surface of

* Presented as Paper IEPC-01-000 at the 27th International Electric Propulsion Conference, Pasadena, CA, 15-19 October, 2001.

thruster, contributes in part a thrust componen[6]. Accordingly, the larger the ratio of power converted into Lorentz work, the higher would be the thrust efficiency, because of less heat loss ratio over total power input. Experiments, numerical and theoretical analyses have been performed on applied-field MPD thrusters of several hundreds kW [6]- [9].

On 1-10 kW class arcjet thrusters, however, the effects of applied field have never been studied. In order to estimate the effects of applied field on plasma in 1-10 kW class arcjet thrusters, we have performed numerical analyses using an axisymmetric 2-D model. This model incorporates (1) finite-rate ionization and recombination processes, and (2) electron temperature nonequilibrium, to correctly capture the phenomena in plasma.

Assumptions

The flowfield and electromagnetic field are simplified under the following assumptions:

1. The flowfield is axisymmetric and viscous: Physical properties have no gradients in azimuthal direction.
2. The gaseous propellant is Argon which is considered as a perfect gas, and plasma is quasi-neutral.
3. The electron temperature is in nonequilibrium with the translational temperature of heavy species.
4. The magnetic field consists only of an applied field with negligible self-induced field. It is of constant magnitude in axial direction along the thruster axis.
5. Only the following single-ionization/recombination processe is considered (therefore, electronic excitations are ignored).
6. The effects of magnetic field on transport phenomena and Hall current are ignored.
7. The radiative energy transfers are ignored.

Fundamental Equations

Conservation equations

The fundamental equations are Navier-Stokes equations extended to chemical and thermal nonequilibrium gases. All fluid dynamic equations
are expressed via an unsteady vector equation in a conservation form.

$$\frac{\partial \mathbf{U}}{\partial t}+\frac{\partial \mathbf{F}}{\partial z}+\frac{\partial \mathbf{G}}{\partial r}=\mathbf{H}+\frac{\partial \mathbf{M}}{\partial z}+\frac{\partial \mathbf{N}}{\partial r}+\mathbf{S}. \qquad (1)$$

$$\mathbf{U}=\begin{bmatrix} r \\ ru \\ rv \\ rw \\ e \\ r_{\mathrm{i}} \\ e_{\mathrm{e}} \end{bmatrix}, \mathbf{F}=\begin{bmatrix} ru \\ ru^2+p \\ ruv \\ ruw \\ (e+p)u \\ r_{\mathrm{i}}u \\ e_{\mathrm{e}}u \end{bmatrix}, \mathbf{G}=\begin{bmatrix} rv \\ ruv \\ rv^2+p \\ rvw \\ (e+p)v \\ r_{\mathrm{i}}v \\ e_{\mathrm{e}}v \end{bmatrix},$$

$$\mathbf{H}=\frac{1}{r}\begin{bmatrix} -rv \\ -ruv+t_{zr} \\ -rv^2+rw^2+t_{rr}-t_{qq} \\ -2(ruw-t_{rq})rw \\ -(e+p)v-q_r+ut_{zr}+vt_{rr}+wt_{qr} \\ -r_{\mathrm{i}}v-i_{ir} \\ -e_{\mathrm{e}}v-q_{\mathrm{e}r} \end{bmatrix},$$

$$\mathbf{M}=\begin{bmatrix} 0 \\ t_{zz} \\ t_{zr} \\ t_{zq} \\ ut_{zz}+vt_{zr}+wt_{zq}-q_z \\ -i_{iz} \\ -q_{\mathrm{e}z} \end{bmatrix},$$

$$\mathbf{N}=\begin{bmatrix} 0 \\ t_{zr} \\ t_{rr} \\ t_{rq} \\ ut_{zr}+vt_{rr}+wt_{rq}-q_r \\ -i_{ir} \\ -q_{\mathrm{e}r} \end{bmatrix},$$

$$\mathbf{S}=\begin{bmatrix} 0 \\ 0 \\ j_q B_z \\ -j_r B_z \\ \mathbf{j}\cdot\mathbf{E} \\ \dot{r}_{\mathrm{i}} \\ \mathbf{j}^2/s-de_{\mathrm{e}} \end{bmatrix}. \qquad (2)$$

The total energy and electron energy per unit volume are defined as

$$e = \frac{p}{g-1} + \frac{r\left(u^2+v^2+w^2\right)}{2} + j_{\mathrm{i}} r_{\mathrm{i}}, \quad (3)$$

$$e_{\mathrm{e}} = \frac{p_{\mathrm{e}}}{g-1}, \quad (4)$$

where the electron kinetic energy is neglected, $g = 5/3$ and $j_{\mathrm{i}} = e_{\mathrm{i}}/m_{\mathrm{A}}$.

The static pressures are defined as

$$p = n_{\mathrm{g}} k_{\mathrm{B}} T_{\mathrm{g}} + p_{\mathrm{e}}, \quad (5)$$

$$p_{\mathrm{e}} = n_{\mathrm{e}} k_{\mathrm{B}} T_{\mathrm{e}}, \quad (6)$$

where $n_{\mathrm{g}} = n_{\mathrm{n}} + n_{\mathrm{i}}$, and $n_{\mathrm{e}} = n_{\mathrm{i}}$ because of the quasi-neutral assumption.

The ion mass diffusion vector and heat flux vector of heavy species are defined as

$$\mathbf{i}_{\mathrm{i}} = -D_{\mathrm{A}} + \nabla r_{\mathrm{i}}, \quad (7)$$

$$q_{\mathrm{g}} = j_{\mathrm{i}} \mathbf{i}_{\mathrm{i}} - k_{\mathrm{g}} \nabla T_{\mathrm{g}}. \quad (8)$$

Taking account of deviation between mass center velocities of electron and heavy species, the heat flux vector is defined in the following form[1]:

$$q_{\mathrm{e}} = -k_{\mathrm{e}} \nabla T_{\mathrm{e}} - \frac{g k_{\mathrm{B}} T_{\mathrm{e}}}{(g-1)e} \mathbf{j}. \quad (9)$$

Total heat flux vector is expressed by adding the heat flux vectors of heavy species and electron:

$$\mathbf{q} = \mathbf{q}_{\mathrm{g}} + \mathbf{q}_{\mathrm{e}}. \quad (10)$$

Electron translational energies are transferred by collisions against heavy species: The rate of its energy transfer is defined as

$$d\,e_{\mathrm{e}} = (n_{\mathrm{en}} + n_{\mathrm{ei}}) n_{\mathrm{e}} k_{\mathrm{B}} (T_{\mathrm{e}} - T_{\mathrm{g}}) + j_{\mathrm{i}} r_{\mathrm{i}}, \quad (11)$$

where the first term is the energy transfer by elastic collision, while the second term by inelastic collision like ionizations and recombinations.

Electromagnetic field equations

In an applied field arcjet, Hall current may be large especially in nozzle, where the plasma is of low density. In the present study, however, Hall current is ignored for simplicity, as the first step to estimate swirl acceleration. The magnetic field consists only of applied field having only a component in axial direction. In addition, by ignoring the term of electron pressure gradient, the generalized Ohm's law is written as follows:

$$\mathbf{j} = s\left(\mathbf{E} + \mathbf{u} \times \mathbf{B}\right). \quad (12)$$

The components of current density are expressed as follows:

$$j_r = s\left(E_r + wB_z\right), \quad (13)$$

$$j_q = -svB_z, \quad (14)$$

$$j_z = sE_z. \quad (15)$$

From Eq.(12) and steady-state Maxwell equations, the following elliptic equation is derived with respect to the electric potential f in the axisymmetric cylindrical coordinates:

$$\frac{\partial}{\partial z}\left(rs\,\frac{\partial f}{\partial z}\right) + \frac{\partial}{\partial r}\left(rs\,\frac{\partial f}{\partial r}\right) = \frac{\partial}{\partial r}\left(rwB_z\right). \quad (16)$$

Transport properties

Because the arcjet has both slightly ionized and highly ionized domains, the transport properties need to be estimated taking account of these two different collision processes. Regarding the electric conductivity, for example,

$$s_{\mathrm{L}} = \frac{n_{\mathrm{e}} e^2}{m_{\mathrm{e}} \sum_j n_{\mathrm{ej}}}, \quad (17)$$

$$s_{\mathrm{H}} = 1.53 \times 10^{-2} \frac{T_{\mathrm{e}}^{3/2}}{\ln \Lambda}\,[\mathrm{S}]. \quad (18)$$

The former is for a slightly ionized plasma based on Chapman-Cowling theory, while the latter is for a highly ionized plasma introduced by L.Spitzer. In the present study, the substantial electric conductivity is defined as in the followin [10]:

$$s = \frac{s_{\mathrm{L}} s_{\mathrm{H}}}{s_{\mathrm{L}} + s_{\mathrm{H}}}. \quad (19)$$

Although other properties related to charged particles are similarly defined, the viscosity of entire fluid is defined by summation among ions and neutrals. Additionally, with regard to the diffusion of ions, the following ambipolar diffusion coefficient is adopted:

$$D_{\mathrm{A}} = \left(1 + T_{\mathrm{e}}/T_{\mathrm{g}}\right) D_{\mathrm{i}}. \quad (20)$$

All the transport properties perpendicular to apllied magnetic field are smaller than the properties parallel to field, because charged particles are captured by field. However, the present model ignores this effect just for simplicity.

Numerical Procedure

Fig.2 shows the schematic picture of grid system for a thruster, which is identical to Nagoya University Arcjet Thruster Second (NUATII). The constrictor of NUATII is considerably long, so that it can effectively use the applied field of solenoidal coil.

In order to save calculation cost, the upstream end of calculation domain is extended up to the upstream end of cathode cone, whereas the downstream end is limited to one third of nozzle length of NUATII, where the flow is adequately supersonic. In the general coordinate system (x, h), the grid points are 165×40, where the cells are clustered near both electrode surfaces, upstream end of constrictor and cathode tip, enabling us to resolve anticipated steep gradients of physical properties. The constrictor radius is 1.0mm, while its length is 10.0mm, and the axial gap between cathode tip and constrictor upstream end is 0.5mm.

The fluid dynamic vector equation transformed to the general coordinate is solved, using the Harten-Yee's 2nd-order-accurate fully-explicit symmetric TVD schem[11], where the time increment is determined by the CFL condition.

On the other hand, the electric field is determined at every time step of flowfield, by solving Eq.(16), using FEM under the assumption that the electric field is steady-state for given flowfield.

Boundary conditions

At inlet boundary, the flow is assumed subsonic. Therefore, one of the independent variables should be determined from downstream. In the present study, the static pressure is determined from downstream by zeroth-order extrapolation for simplicity. At inlet, the mass flow rate is specified as the operating parameter of experiment, the total enthalpy is specified to 300K, and the azimuthal velocity is set to zero in order to purely evaluate subsequent swirl acceleration by applied field. The number densities of charged particles are set to zero, while the electron temperature is set equal to the heavy species temperature. Then, the velocity, density, and temperature are obtained from the energy conservation law, using the above-mentioned values.

At exit boundary, the flow is assumed supersonic by neglecting the influence of subsonic region near anode wall. Therefore, physical properties are determined from upstream by zeroth-order extrapolation.

On the electrode surfaces, the viscous non-slip condition is naturally imposed: The normal gradient of static pressure is set to zero. The normal gradients of both electron temperature and number densities of charged particles are also set to zero. In other words, the electrode surfaces are assumed non-catalytic. Therefore, the detailed physical aspects near electrodes are ignored. The cathode wall temperature is set to increase linearly from 300K at inlet, up to 3600K at cathode tip. The anode wall temperature is set to increase linearly from 300K at inlet, up to 1600 K at upstream end of constrictor. The constrictor wall temperature is kept at a constant value, 1600K. On the other hand, the anode wall temperature is set to decrease linearly form this value down to 500K at the end of nozzle. Such temperatures of both electrodes are fixed throughout calculation. On the electrode surfaces, the temperatures of heavy species are assumed to immediately accomodate with the electrode temperature. Along the center axis, the axisymmetric condition stating that both azimuthal and radial velocity components are zero, is imposed. The normal gradients of other physical properties are set to zero.

With regard to the boundary conditions on electric field, the discharge voltage is imposed on cathode surface as a negative potential in comparison with anode. This cathode potential is controlled to satisfy the condition that the calculated total discharge current is equal to the given value of operating parameter. At inlet, along center axis and at exit boundary, the natural boundary condition for potential is satisfied.

Results and Discussion

Calculations are conducted for the three cases: The applied field $B = 0.00$T, 0.25T and 0.50T, with the total discharge current $J =$ 80A and the mass flow rate $\dot{m} = 0.1$g/s.

Case for no applied field

The current streamlines for Case $B = 0.00$T are shown in Fig.3, where the arc current streamlines attach to the anode surface between the middle of cathode and the vicinity of constrictor upstream end; the discharge mainly occurs in this region. Thus, we hereafter refer this region as "the discharge region". This result shows that the thruster is operated in low voltage mode, which agrees with numerous existing experiments and calculations using Argon as propellant.

Cases with applied magnetic fields

The contours of azimuthal velocity for Case $B = 0.50$ T is shown in Fig.4. The maximum velocities are $w = 912.4$m/s and 1168.6m/s for Cases $B = 0.25$T and 0.50T, respectively. The axial profiles of azimuthal velocity and azimuthal Lorentz force $j_r B_z$, between the inlet and middle of constrictor, are shown in Figs.5 and 6. As the arc discharge has nearly ended downstream of constrictor inlet, which is identical to Case $B = 0.00$T, the azimuthal acceleration by Lorentz force also ends once the flow enters constrictor inlet. In the constrictor region, the azimuthal velocity gradually decreases due to viscous effect from constrictor wall. However, the rate of decrease becomes slower with approach to constrictor wall, because the azimuthal momentum is transferred to radial direction by viscous momentum transfer from center line region where the azimuthal velocity is maximum.

In order to estimate how the input power is used as Lorentz work per unit volume, we introduce the following ratio:

$$h_{\mathrm{L}} \equiv \frac{\text{Lorentz work per unit volume}}{\text{Input power per unit volume}} = \frac{\left| w j_r B_z \right|}{\mathbf{j} \cdot \mathbf{E}}. \quad (21)$$

Figure.7 shows the radial profiles of h_{L} between the cathode tip and the constrictor upstream corner. When the applied magnetic fields are stronger, h_{L} becomes higher. For Cases $B = 0.25$T and 0.50T, the maximum values of h_{L} are about 2% and 7%, respectively. Thus, it is concluded that the input power is reasonably well transformed to Lorentz work.

Performance estimation with applied fields

In order to estimate the effect of applied fields on thruster performance, the following ratios are defined:

The Lorentz efficiency

$$h_{\mathrm{Loverall}} \equiv \frac{\text{Overall Lorentz work in thruster}}{\text{Total input power}} = \frac{\int \left| w j_r B_z \right| dv}{VJ}. \quad (22)$$

The thrust efficiency

$$h_{\mathrm{T}} \equiv \frac{\text{Axial thrust energy}}{\text{Total input power} + \text{inflow enthalpy}} = \frac{T^2 \int \left| w j_r B_z \right| dv}{2\dot{m}\left(VJ + \dot{m}H_0\right)}. \quad (23)$$

h_{Loverall} is shown in Fig.8, while h_{T} and axial thrust are shown in Fig.9. h_{Loverall} for Case $B = 0.50$T is about three times as high as h_{Loverall} for Case $B = 0.25$T. Thus, such evaluation of h_{Loverall} also proves the effectiveness of applied field.

The thrust and h_{T} also increase with increased applied fields, as shown in Fig.9. Figure.10 shows the distribution of azimuthal kinetic energy integrated over the cross-section normal to x direction, between slightly upstream of constrictor downstream end and nozzle end. Although the azimuthal kinetic energy for Case $B = 0.50$T is higher than Case $B = 0.25$T at constrictor downstream end, the azimuthal kinetic energies for both Cases become nearly identical at zero level at nozzle end, implying that the azimuthal kinetic energy is adequately transformed to axial kinetic energy by solid nozzle.

With regard to the estimation of heat loss to anode, the most important factor is the anode heat flux due to wall bombardment of electron from discharge current.

Accordingly, such heat flux carried by discharge current can be evaluated only by the following quantity:

$$h_{\mathrm{Q}} \equiv \frac{\text{Total heat flux to anode by current}}{\text{Total input power} + \text{inflow enthalpy}} = \frac{\int_{\text{anode wall}} \frac{g\, k_{\mathrm{B}} T_{\mathrm{e}}}{(g-1)e} \sqrt{j_r^{\,2} + j_z^{\,2}}\, dS}{\left(VJ + \dot{m}H_0\right)}. \quad (24)$$

h_{Q} is shown in Fig.11, where although h_{Q} decreases with increasing applied field, the decreasing rate is not very high because the total current is fixed as an operating parameter. To estimate the dependence of heat flux distribution along anode on applied field, the following dimensionless quantity h_{q} is introduced, of which the value in discharge region and its magnified picture near constrictor upstream end are shown in Fig.12:

$$h_{\mathrm{q}} = \frac{\left[2\pi r_{\mathrm{a}} \frac{g\, k_{\mathrm{B}} T_{\mathrm{e}}}{(g-1)\mathrm{e}} \sqrt{j_r^{\,2} + j_z^{\,2}} \right] R_{\mathrm{c}}}{\mathrm{VJ}}. \quad (25)$$

Here r_{a} is the anode radius and r_{c} is the constrictor radius which is used as the reference length for non-dimensionalization. h_{q} for each applied field has a peak at constrictor upstream end. The peak value of

h_q becomes lower for a stronger applied field, because the counter-electromotive force, wB_z in Eq.(13), increases for an increased applied field near constrictor upstream end.

Consequently, these results on efficiency indicate the improvement of thrust performance by applying magnetic field. However, the decrease in azimuthal velocity in constrictor prevents even better improvement which would have been given by applied field. Since the arc discharge is occurring near constrictor upstream end in low voltage mode, a long constrictor used in the present study under the intention of efficient usage of applied field, has turned out to be inappropriate. In conclusion, therefore, a shorter constrictor seems to improve the thrust performance more effectively.

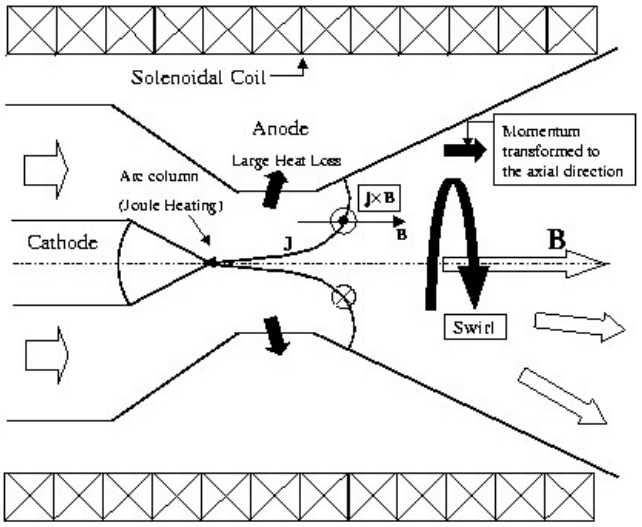

Figure 1 Acceleration mechanism of applied-field arcjet.

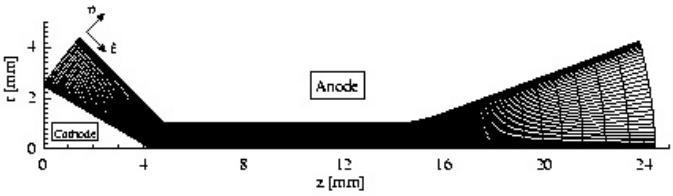

Figure 2 Thruster geometry and grids (165×40).

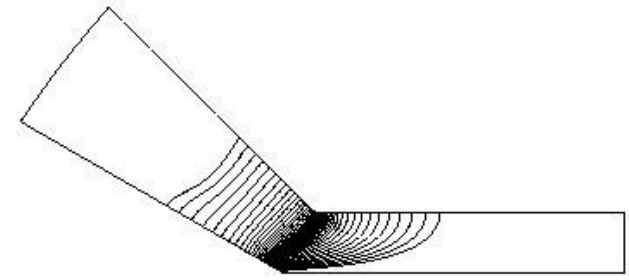

Figure 3 Current streamlines in discharge region for no applied field.

Figure 4 Azimuthal velocity contours for Case B = 0.50T.(max.= 1168.6m/s, min.= 0.0m/s, increment= 100.0m/s)

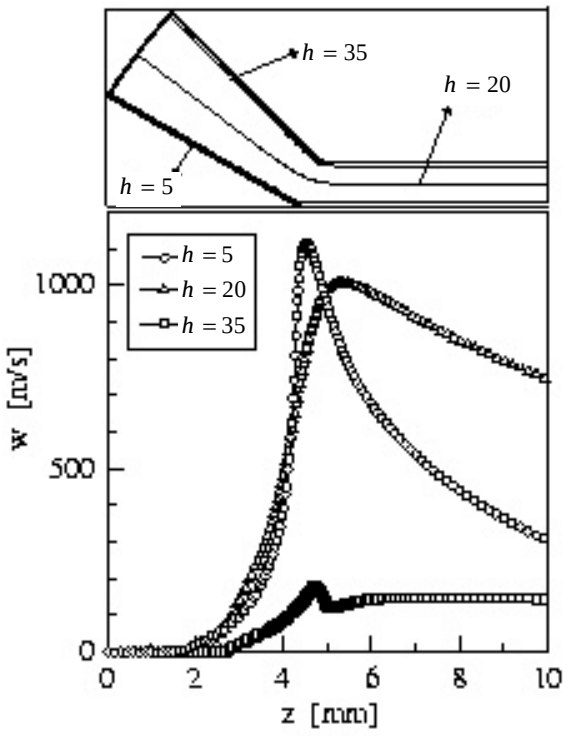

Figure 5 Azimuthal velocity profiles between inlet and middle of constrictor for Case B = 0.50T.

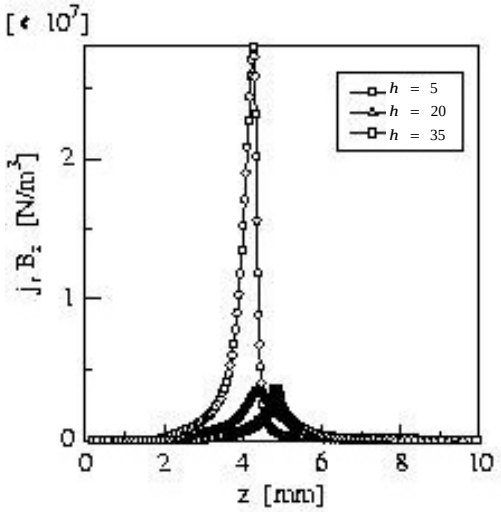

Figure 6 Lorentz force profiles between inlet and middle of constrictor for Case $B = 0.50$T.

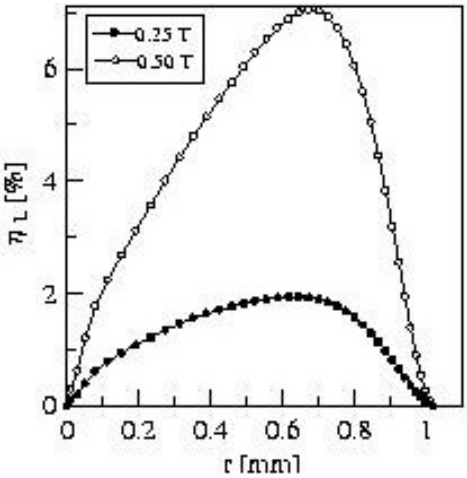

Figure 7 Radial profiles of h_{L} between cathode tip and constrictor upstream corner.

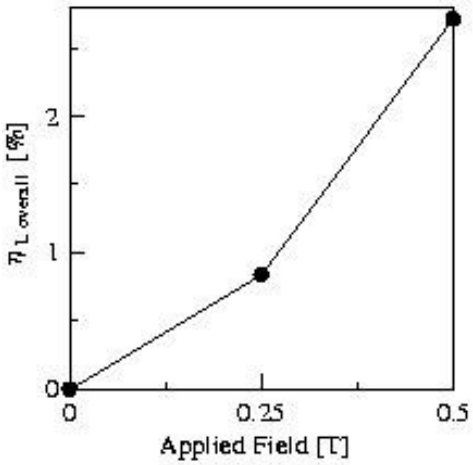

Figure 8 Lorentz efficiency for entire thruster.

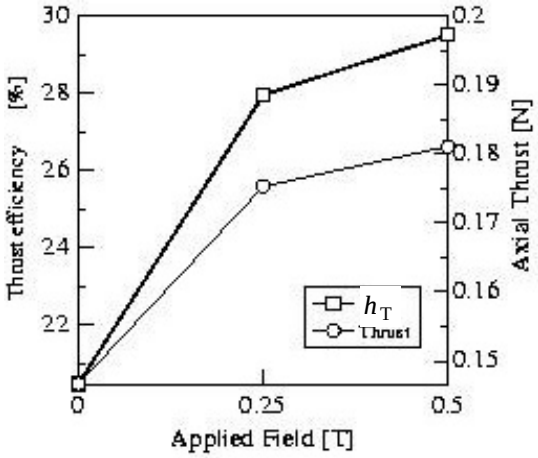

Figure 9 Thrust efficiency and thrust vs. applied field.

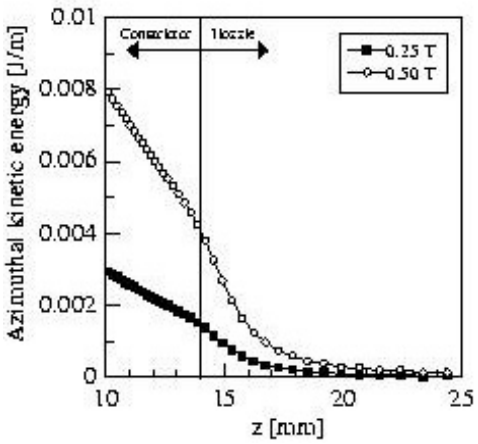

Figure 10 Distribution of azimuthal kinetic energy integrated over cross-section normal to x direction, between slightly upstream of constrictor downstream end and nozzle end.

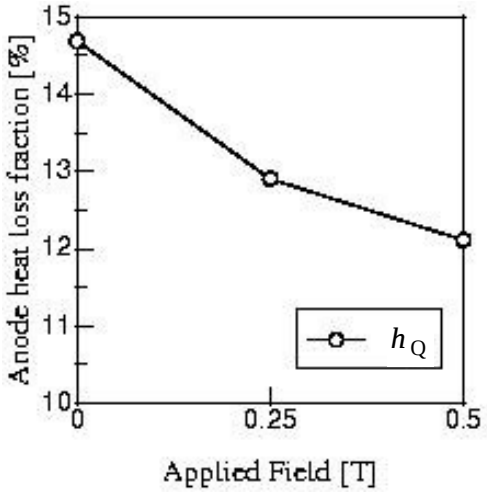

Figure 11 Anode heat loss caused by wall bombardment of electron from discharge current.

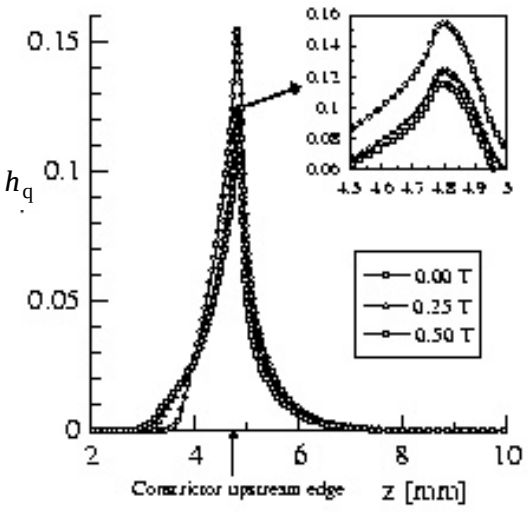

Figure12 Profiles of h_q in discharge region and magnified picture near constrictor upstream end.

Conclusion

Numerical results show that plasma is adequately accelerated to azimuthal direction by applied field, as was intended intially.

The effects of applied magnetic field on thruster performance are evaluated in terms of thrust and thrust efficiency. It is found out that the thruster performance is improved by applied field. In order to improve the performance more significantly, however, the idea to apply a stronger field to a thruster with shorter constrictor seems to be more effective.

Speaking in more detail, the applied field would become more effective for high voltage mode than for low voltage mode, because the azimuthal acceleration would occur in nozzle; the azimuthal momentum would be quickly transformed to axial momentum by the current streamlines stretched down to nozzle.

In future, we will focus our efforts on the applied-field arcjet having high voltage mode and shorter constrictor.

References

[1] Fujita, K., "Performance Computation of a Low-Power Hydrogen Arcjet,"
AIAA Paper 96-3183, July 1996.

[2] Kuchi-ishi, S., and Nishida, M., "Thermo-chemical Nonequilibrium Modeling for a Nitrogen Arcjet Thruster,"Proceedings of the 26th International Electric Prolulsion Conference, Kitakyushu, Japan, 1999, 99-029, pp.193-200.

[3] Kuchi-ishi, S., and Nishida, M., "Numerical Simulation of a Nitrogen Arcjet Thruster,"Transactions of the Japan Society for Aeronautical and Space Sciences, Vol.42, No.136, 1999, pp.69-75.

[4] Auweter-Kurtz, M., Gölz, T., Habiger, H., Hammer, F., Kurtz, H., Riehle, M., and Sleziona, C., "High-Power Hydrogen Arcjet Thrusters,"Journal of Propulsion and Power, Vol.14, No.5, Sep-Oct, 1998.

[5] Miller, S. A., Martinez-Sanchez, M., "Two-Fluid Nonequilibrium Simulation of Hydrogen Arcjet Thrusters,"Journal of Propulsion and Power, Vol.12, No.1, Jan-Feb, 1996.

[6] Sasoh, A., and Arakawa, Y., "Thrust Formula for an Applied MPD Thruster Derived from Energy Conservation Equation,"Proceedings of the 22nd International Electric Prolulsion Conference, Viareggio, Italy, 91-062, 1991.

[7] Thomas, H., Chapman, R., and Garrison, G. W., "A Numerical Simulation of Axisymmetric, Steady-State Plasma Flow Through MPD-Type Thrusters With Applied Magnetic Fields,"
AIAA Paper 92-3737, 1992.

[8] Tanaka, M., and Kimura, I., "Current Distribution and Plasma Acceleration in MPD Arcjets with Applied Magnetic Fields,"Jornal of Propulsion and Power, Vol.4, No.5, Sep-Oct. 1988. pp.428-436.

[9] Myers, R.M., "Scaling of 100 kw Class Applied-Field MPD Thrusters,"AIAA Paper 91-3462, July 1992.

[10] Cambel, A.B., "Plasma Physics and Magnetofluidmechnics,"McGraw-Hill Book Company, New York, pp152-195, Chap.7, 1963.

[11] Yee, H.C., "A Class of High-Resolution Explicit and Implicit Shock-Capturing Methods,"NASA-TM 101088, 1989.